PHYSICAL REVIEW B **93**, 094422 (2016)

Large adiabatic temperature and magnetic entropy changes in $EuTiO_3$

A. Midya and P. Mandal
Saha Institute of Nuclear Physics, 1/AF Bidhannagar, Calcutta 700064, India

Km. Rubi, Ruofan Chen, Jiang-Sheng Wang, and R. Mahendiran*
Physics Department, National University of Singapore, 2 Science Drive 3, Singapore 117551, Republic of Singapore

G. Lorusso and M. Evangelisti
Instituto de Ciencia de Materiales de Aragón (ICMA) and Departamento de Fisica de la Materia Condensada, CSIC-Universidad de Zaragoza, 50009 Zaragoza, Spain

(Received 24 August 2015; revised manuscript received 9 January 2016; published 16 March 2016)

We have investigated the magnetocaloric effect in single and polycrystalline samples of quantum paraelectric $EuTiO_3$ by magnetization and heat capacity measurements. Single crystalline $EuTiO_3$ shows antiferromagnetic ordering due to Eu^{2+} magnetic moments below $T_N = 5.6$ K. This compound shows a giant magnetocaloric effect around its Néel temperature. The isothermal magnetic entropy change is 49 J kg^{-1}K^{-1}, the adiabatic temperature change is 21 K, and the refrigeration capacity is 500 J kg^{-1} for a field change of 7 T at T_N. The single crystal and polycrystalline samples show similar values of the magnetic entropy and adiabatic temperature changes. The large magnetocaloric effect is due to suppression of the spin entropy associated with the localized $4f$ moment of Eu^{2+} ions. The giant magnetocaloric effect, together with negligible hysteresis, suggest that $EuTiO_3$ could be a potential material for magnetic refrigeration below 40 K.

DOI: 10.1103/PhysRevB.93.094422

I. INTRODUCTION

Refrigeration has become an essential technology in our modern society. However, traditional gas compression refrigerators which use ozone depleting volatile refrigerants such as chlorofluorocarbons (CFCs) and hydrochlorofluorocarbons (HCFCs) are reaching their technical boundaries in achieving further improvements [1,2]. Therefore, in addition to further developing gas compression technology, scientists and engineers have begun to explore alternative environmentally friendly and energy-efficient cooling technologies to replace conventional gaseous refrigeration. Magnetic refrigeration can provide such an opportunity. This technology exploits the magnetocaloric effect (MCE) in a solid-state magnetic refrigerant, i.e., the change of the adiabatic temperature (ΔT_{ad}) and isothermal magnetic entropy (ΔS) of the functional material upon applying or removing an external magnetic field. The mainstream in this field is to find new materials exhibiting a large MCE close to room temperature for domestic and industrial uses. However, low-temperature refrigeration is important not only for basic research but also for cooling superconducting magnets used in magnetic resonance imaging and liquefaction of hydrogen in the fuel industry [1,3]. Although ΔS can be large for first-order phase transitions in which magnetic and structural transitions are strongly coupled [4,5,6], there are challenges associated with the thermal hysteresis and mechanical instability of these compounds. Hence, new materials exhibiting a second-order phase transition with negligible hysteresis and large MCE are still being widely explored [7].

Materials containing Eu^{2+} ($4f^7$) and Gd^{3+}($4f^7$) ions can show a large isotropic magnetocaloric effect since these two ions have a large total angular momentum ($J = S = 7/2$ and $L = 0$). In this context, $EuTiO_3$ is interesting since it has a divalent Eu ion with a large magnetic moment and a tetravalent Ti ion with no magnetic moment. $EuTiO_3$, a G-type antiferromagnet below $T_N = 5.5 \pm 0.2$K [8,9], has attracted much attention in recent years due to the observations of a magnetodielectric effect in single crystals [10], tensile strain-induced ferromagnetism and ferroelectricity in thin films [11], and magnetoelastic properties [12,13]. It is also unique among the rare earth titanates ($RTiO_3$, where R is the rare earth ion) because only the Eu^{2+} ion adopts a divalent state instead of a trivalent state that is adopted by other rare earth ions (R = Gd, Y, etc.). Recently, polycrystalline samples of $Eu_{1-x}Ba_xTiO_3 (0.1 \leqslant x \leqslant 0.9)$ [14], $EuTiO_3$ [15], and $EuTi_{1-x}Cr_xO_3$ [16] were studied from the perspective of the magnetocaloric effect and were found to show a huge isothermal magnetic entropy change ($\Delta S \sim 45-40$ J kg^{-1} K^{-1} for $x = 0.0-0.1$), as estimated from magnetization isotherms. It is of paramount importance that a good magnetic refrigerant possess not only a large ΔS value, but also a large adiabatic temperature change (ΔT_{ad}) and refrigeration capacity (RC) in relative low magnetic fields. In this paper, we report $\Delta S, \Delta T_{ad}$, and RC in single crystalline as well as polycrystalline $EuTiO_3$ samples. The magnetocaloric study in the polycrystalline sample was extended down to 350 mK, while 2 K was the lowest temperature used for the single crystal. We also calculated the magnetization and magnetic entropy change using a mean field treatment of the Heisenberg model and fitted with experimental data of single crystal $EuTiO_3$.

II. EXPERIMENTAL DETAILS

Polycrystalline $EuTiO_3$ samples were prepared by the solid-state reaction method using preheated Eu_2O_3 and TiO_2 in a reduced atmosphere (5%H_2 and 95% Ar), independently

*Corresponding author: phyrm@nus.edu.sg

at the National University of Singapore (NUS) and the Saha Institute of Nuclear Physics (SINP), India. The single crystal was grown by the traveling solvent floating zone technique using an image furnace (NEC) under a reduced atmosphere at SINP. The x-ray diffraction pattern of the powdered sample of the single crystal reveals that the compound is single phase with a cubic structure ($Pm3m$ space group) at room temperature. The dc magnetization was measured using a vibrating sample magnetometer. A magnetic field was applied along the [001] axis of the crystal. The heat capacity of the single crystal sample down to 2 K was measured by a relaxation technique in a physical property measurement system (PPMS, Quantum Design). Apiezon N grease was used between the sample and the base for good thermal contact for temperatures below 200 K. Since Apiezon N grease gave a spurious signal around 280 K, the measurement above 200 K was done with Apiezon H grease, which does not give a spurious signal [17]. The heat capacity from 50 K down to 300 mK on the polycrystalline sample was also measured in a PPMS equipped with the ^{3}He option, available at ICMA, University of Zaragoza. The polycrystalline sample consisted of thin pressed pellets (~1 mg) thermalized with ~0.2 mg of Apiezon N grease, whose contribution was subtracted using a phenomenological expression. The temperature dependence of entropy (S) at a constant field H is estimated directly from the heat capacity at a constant pressure (C_p), measured under a magnetic field H using the relation $S(H,T) = \int_{T_1}^{T_2} \frac{C_p(H,T)}{T} dT$, where T_1 and T_2 are the lowest and highest temperatures of interest. $\Delta S(H,T) = S(H=0,T) - S(H,T) = \int_{T_1}^{T_2} \frac{C_p(0,T) - C_p(H,T)}{T} dT$ is the total entropy change obtained upon changing the magnetic field from zero to H. The entropy change as the field is changed from an initial value H_1 to a final value H_2 is also obtained from magnetization versus magnetic field isotherms using a numerical approximation to the Maxwell relation $\Delta S(H,T) = \int_{H_1}^{H_2} (\frac{\partial M}{\partial T})_H dH$.

III. RESULTS AND DISCUSSION

The left y axis of Fig. 1(a) shows the temperature dependence of the zero-field-cooled (ZFC) and field-cooled (FC) dc susceptibility $\chi_{dc} = M/H$ of single crystalline $EuTiO_3$ in a low-temperature region ($T = 2-50$ K) under $H = 100$ Oe. No significant difference was observed between the ZFC and FC curves. The dc susceptibility increases sharply with decreasing temperature and shows a peak at $T_N = 5.6$ K, which corresponds to antiferromagnetic (AFM) ordering of Eu^{2+} moments. We also plotted the inverse susceptibility $1/\chi_{dc}$ on the right y axis over a broad temperature range ($T = 400-2$ K) and it follows the Curie-Weiss (CW) law $\chi = C/(T-\theta_{cw})$. A linear fit to high temperature yields a Curie constant ($C = 7.73$ emuK/mol Oe) and a positive Curie-Weiss temperature $\theta_{CW} = 3.1$ K. The value of θ_{CW} is consistent with the previously reported result [13]. The effective moment estimated from the relation $P_{eff} = (\frac{3k_B C}{N})^{1/2}$ is 7.86 μ_B, which is very close to the theoretically expected value of $P_{eff} = 2\sqrt{J(J+1)}\mu_B = 7.94\ \mu_B$ corresponding to the $4f^7$ spin configuration of Eu^{2+} ($J = 7/2$). Figure 1(b) displays the temperature dependence of the specific heat (C_p) of the $EuTiO_3$ crystal. While overall C_p decreases with

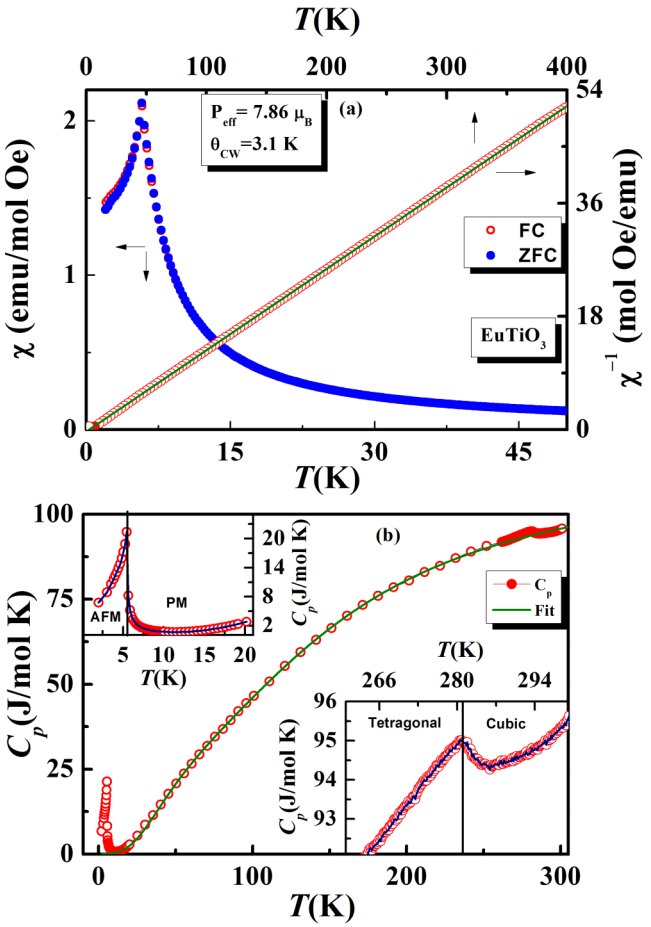

FIG. 1. (a) Temperature dependence of dc magnetic susceptibility (χ) of single crystalline $EuTiO_3$ under field- cooled (FC) and zero-field-cooled (ZFC) processes (left y axis) and inverse susceptibility as a function of temperature (right y axis and top x axis). The symbol and solid line represent the experimental data and Curie-Weiss fit. (b) Temperature dependence of zero-field heat capacity (C_p). The upper and lower insets show the heat capacity curve around magnetic and structural phase transitions, respectively.

lowering temperature from 300 K, two prominent anomalies occur, one near room temperature and another below 10 K, as shown in the lower and upper insets. The high-temperature peak in C_p around 281 K is now known to be due to a structural transition from a cubic to tetragonal phase [18] and the sharp peak around 5.6 K is due to antiferromagnetic ordering of $4f^7$ spins of Eu^{2+} ions. The temperature dependence of the heat capacity for $T = 20-250$ K can be fitted well with the combined Debye plus Einstein models [19].

In order to investigate the influence of applied magnetic field on the magnetic ground state, we have also measured the field dependence of magnetization (M) in the neighborhood of the magnetic transition and beyond. Some representative plots of the field dependence of magnetization for $EuTiO_3$ are presented in Fig. 2(a). A qualitatively similar behavior has been observed in polycrystalline $Eu_{1-x}Ba_xTiO_3$ for $0.1 \leqslant x \leqslant 0.9$ compounds [14]. Below T_N, M varies almost linearly with magnetic field up to a critical field H_C, above which it shows a tendency to saturate. The critical field H_C indicates

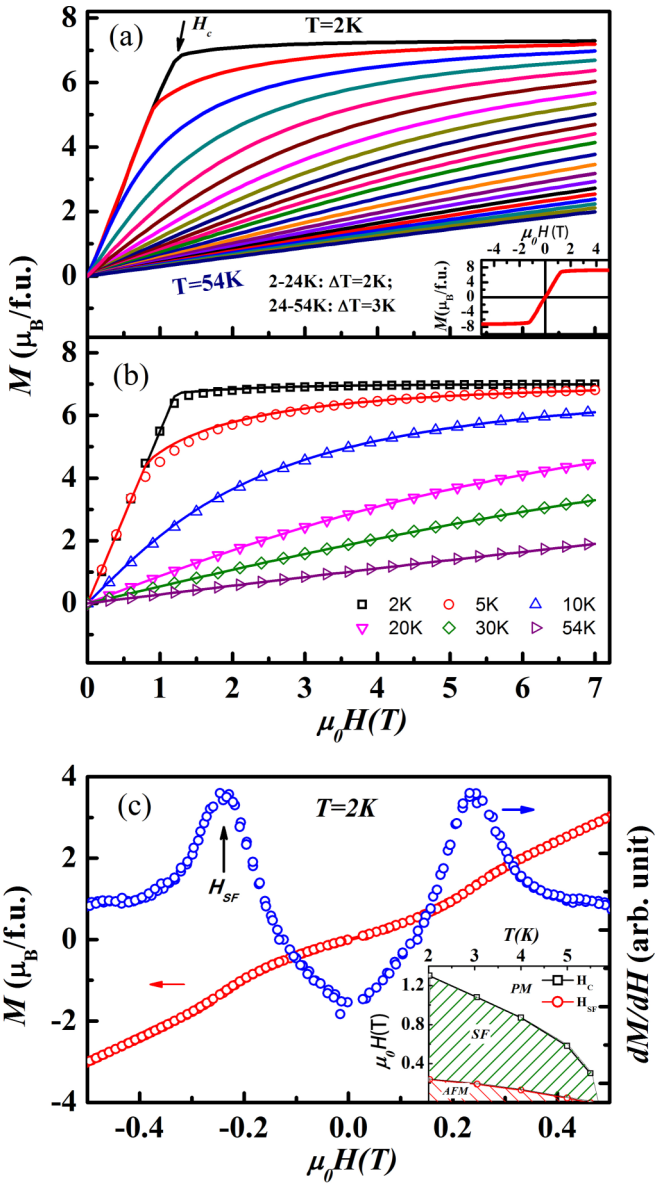

FIG. 2. (a) Isothermal magnetization curves for $EuTiO_3$ single crystal. H_C is the critical field for the spin-flopped antiferromagnetic phase to a field-induced ferromagnetic state. Inset: The five-segment magnetization curve at 2 K. (b) Experimental *M-H* data (symbol) and theoretical fit (line) using Eq. (A10) in the Appendix. (c) Main panel: Expanded view of low-field magnetization at 2 K (left *y* axis) and the derivate *dM/dH* (right *y* axis). H_{SF} is the critical field for the spin-flop transition. The inset shows the plot of H_{SF} and H_C as a function of temperature.

a transition from a spin-flopped antiferromagnetic phase to a field-induced ferromagnetic phase or paramagnetic phase. At $T = 2$ K and $\mu_0 H = 7$ T, the observed value of M is $7.0\,\mu_B$ per formula unit for $EuTiO_3$, which exactly matches with $M_S = g\mu_B S = 7\,\mu_B$, expected for complete alignment of all Eu^{2+} spins. Thus, the Eu:$4f^7$ spins are completely spin polarized at 7 T. Above T_N, M increases smoothly with magnetic field following the Brillouin function. The inset of Fig. 2(a) displays $M(H)$ measured at $T = 2$ K for $\mu_0 H = 0 \rightarrow +7$ T $\rightarrow -7$ T $\rightarrow +7$ T. Hysteresis is not observed, even at low magnetic fields. von Ranke *et al.* calculated the magnetization and magnetic entropy change in $EuTiO_3$ using a mean field treatment of the Heisenberg model [20]. We followed their approach and calculated the magnetization isotherms at selected temperatures using Eq. (A10) in the Appendix. We plot the experimental and calculated data together in Fig. 2(b). We used $J_1/k_B = -0.0407$ K and $J_2/k_B = 0.0828$ K, $g = 2$, where J_1 and J_2 are the nearest neighbor and next nearest neighbor exchange interactions, and g is the gyromagnetic ratio. The calculated data (solid line) and experimental data (symbol) match perfectly for all temperatures and magnetic field except at $T = 5$ K near field 1 T. These remarkably accurate fittings are achieved by adjusting the J_1 and J_2 values 10% and 20% higher, respectively, than the values used by Katsufuji and Takagi [10]. The reason for this is that Katsufuji and Takagi used mean field theory predictions of T_N and θ_{CW} to uniquely determine J_1 and J_2. However, mean field theory typically overestimates the value of T_N. Figure 2(c) allows us to have a closer look at the magnetization curve within the antiferromagnetic state at $T = 2$ K. As can be seen, M shows a feeble but clearly visible steplike increase around 0.2 T. This step represents the spin-flop transition of the antiferromagnetic sublattices. The position of the peak in the dM/dH curve is taken as the critical field H_{SF} for the spin-flop transition. As the field increases above H_{SF}, the sublattice magnetization gradually cants towards the direction of the magnetic field and they become aligned along the field direction above the critical field H_C. We show the temperature variation of H_{SF} and H_C in the inset of Fig. 2(c). Both of them go to zero at T_N. The small value of H_{SF} suggests that anisotropy is weak in $EuTiO_3$.

The isothermal entropy change was obtained from the $M(H)$ isotherms using the Maxwell relation $-\Delta S(T,H) = \sum_i \frac{M_{i+1}(T_{i+1},H_i) - M_i(T_i,H_i)}{T_{i+1}-T_i}\Delta H_i$, where M_i and M_{i+1} are the magnetizations measured at T_i and T_{i+1} temperatures, respectively, for magnetic field H_i. S comprises structural, electronic, and magnetic entropies. The investigated compound is an insulator and does not show any structural transition below 40 K. Hence, ΔS represents the magnetic entropy change alone in this sample. The thermal variations of the entropy change ΔS for different magnetic fields are shown in Fig. 3(a) with theoretical estimates of ΔS from the mean field model using Eqs. (A12) and (A13) in the Appendix. The curves present a characteristic shape with a maximum near the antiferromagnetic ordering temperature T_N. While the calculated data using the mean field treatment exactly follow the experimental data in the paramagnetic region, a slight deviation has been observed around T_N. The sign of ΔS is negative down to the lowest temperature and the maximum value of ΔS increases with the field reaching a value 49 J kg^{-1} K^{-1} for a field change of 7 T. The refrigerant capacity (RC) is an important quality factor for practical considerations of a magnetic refrigerant material, and it is a measure of the amount of heat transfer between the cold and hot reservoirs in an ideal refrigeration cycle. It is defined as $RC = \int_{T_1}^{T_2} \Delta S dT$, where T_1 and T_2 are the temperatures corresponding to both sides of the half-maximum value of the $\Delta S(T)$ peak. The inset of Fig. 3(a) shows the variation of RC with magnetic field. The RC increases nonlinearly with magnetic field and reaches a value of 500 J kg^{-1} for $\mu_0 \Delta H = 0$–7 T. The adiabatic temperature change $\Delta T_{ad} = T_i - T_f$ is

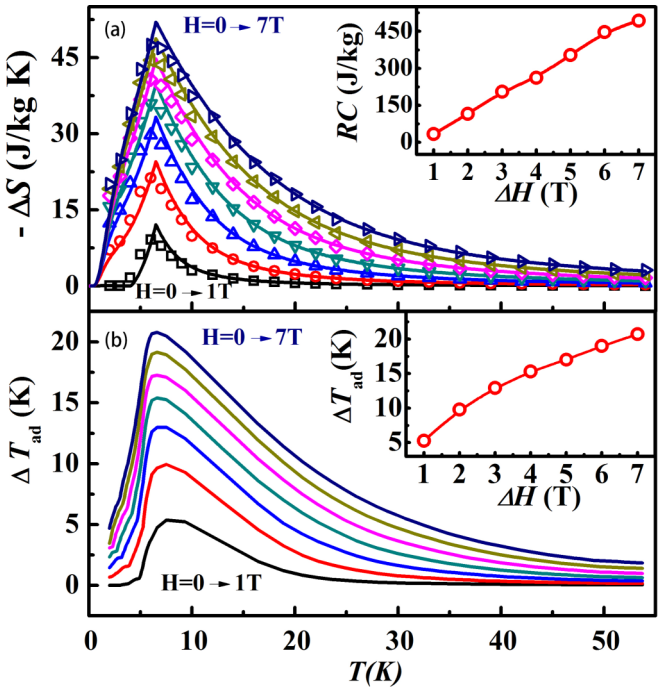

FIG. 3. (a) Temperature dependence of isothermal magnetic entropy change ($-\Delta S$) for $EuTiO_3$ single crystal. Symbols: $-\Delta S$ calculated from isotherm magnetization data; solid lines: $-\Delta S$ calculated from mean field theory. Inset: Refrigeration capacity (RC) as a function of magnetic field. (b) Temperature dependence of the adiabatic temperature change (ΔT_{ad}) for $EuTiO_3$ single crystal. Inset: Magnetic field dependence of the maximum value of ΔT_{ad}.

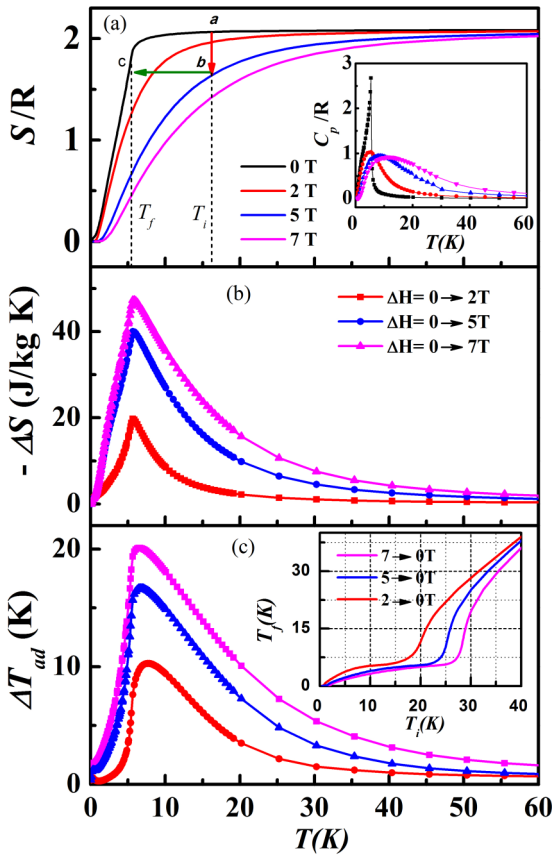

FIG. 4. (a) Main panel: Temperature dependence of magnetic entropy (S) of the polycrystalline $EuTiO_3$ sample calculated from the heat capacity data. Data are shown in symbols and lines are a guide to the eye. The inset shows the temperature dependence of the heat capacity under different fields. (b) Magnetic entropy change ($-\Delta S$) and (c) adiabatic temperature change (ΔT_{ad}) for the polycrystalline $EuTiO_3$ sample. Inset: Final temperature T_f as a function of initial temperature T_i in the adiabatic demagnetization process for different values of the magnetic field.

the temperature change from the initial temperature T_i to the final temperature T_f caused by the intrinsic magnetocaloric effect. $T_f > T_i$ in the adiabatic magnetization process and $T_f < T_i$ in the adiabatic demagnetization process. ΔT_{ad} can be calculated from either the heat capacity measured in zero and nonzero magnetic fields alone or from combined data of the heat capacity in zero field [$C_p(0,T)$] and the magnetic entropy change (ΔS) obtained from $M(H)$ isotherms. For the single crystal shown in Fig. 3(b), ΔT_{ad} was estimated by making use of $C_p(0,T)$ and $\Delta S(H,T)$ obtained from magnetization measurements. First, the entropy in zero field was estimated using the relation $S(0,T) = \int_{T_1}^{T_2} \frac{C_p(0,T)}{T} dT$, where T_1 and T_2 are the lowest and highest temperatures of interest. Then, the entropy $S(H,T)$ for a field H was calculated by subtracting the $|\Delta S(H,T)|$ from $S(0,T)$ isothermally. Finally, ΔT_{ad} is obtained from the isentropic line connecting $S(H,T_i)$ and $S(0,T_f)$. The temperature dependence of ΔT_{ad} for a magnetic field change from zero to a final value H is shown in Fig. 3(b). The maximum value of ΔT_{ad} increases monotonically with increasing field and reaches 21 K for $\mu_0 \Delta H = 0-7$ T [see the inset of Fig. 3(b)].

To compare the magnetocaloric properties of single and polycrystalline samples, we measured the heat capacity of the polycrystalline $EuTiO_3$ sample as a function of temperature from 100 K to 350 mK under $\mu_0 H = 0,2,5$, and 7 T. For clarity, we show only the low-temperature data as C_p/R, where R is the gas constant in inset of Fig. 4(a). The zero-field data show a peak at $T = 5.4$ K, which is slightly lower than that of the single crystal ($T_N = 5.6$ K). The heat capacity peak decreases in amplitude, becomes rounded in shape, and shifts towards higher temperature as the external magnetic field increases. The main panel of Fig. 4(a) shows the normalized magnetic entropy (S/R) calculated from the heat capacity data under different magnetic fields. For temperatures above 8 K, S/R approaches a temperature independent value of 2.08, which is the same as the maximum magnetic entropy [$S/R = \ln(2S+1) = \ln(8) = 2.079$] expected for complete randomization of $4f$ spins. The zero-field magnetic entropy drops rapidly below T_N and S decreases in value with increasing magnetic field strength. The entropy change (ΔS) and the adiabatic temperature change (ΔT_{ad}) for the polycrystalline sample are shown in Figs. 4(b) and 4(c), respectively, for field changes of $\mu_0 \Delta H = 2,5$, and 7 T. The ΔT_{ad} shown in Fig. 4(c) are obtained from the heat capacity measurement alone. The values of $-\Delta S$ and ΔT_{ad} in the polycrystalline sample are 40 (47.32) J kg^{-1} K^{-1} and 16.6 (20) K for $\mu_0 \Delta H = 0 \rightarrow 5$ T($0 \rightarrow 7$ T), which are comparable to the values obtained for the single crystal. The ΔT_{ad} plotted here indicates the temperature rises upon adiabatic magnetization. The

TABLE I. Maximum values of $-\Delta S, \Delta T_{ad}$, RC, and magnetic transition temperature for $EuTiO_3$ with other potential magnetic refrigerant materials. SC: single crystal; PC: polycrystal.

Compound	ΔT_{ad}(K)	ΔS(J/kg K)	RC (J/kg)	$\mu_0 \Delta H(T)$	T_N/T_C(K)	Reference
$EuTiO_3$(SC)	16.6	42.4	353	5	5.6	This work
$EuTiO_3$(PC)	16.5	40.4	300	5	5.4	This work
$Eu_{0.9}Ba_{0.1}TiO_3$		40		5	3.47	[14]
$DyTiO_3$		16	360	5	64	[21]
EuO	6.8	17.5		5	69	[22]
Eu_3O_4	7.8	12.7		5	5.3	[23]
EuSe		37.5	435	5	4.6	[24]
$EuHo_2O_4$	11.6	22.5	260	5	5	[25]
$ErAl_2$	12	36		5	13	[26]
$Gd_3Ga_5O_{12}$	24	25		5	1	[27]
$Gd_3Al_5O_{12}$		29		5		[28]
$Gd(HCOO)_3$	22	55		7	2	[29]

dependence of the final temperature (T_f) that can reachable by an adiabatic removal of magnetic field at temperature T_i is more intuitive and it is shown in the inset of Fig. 4(c). If the sample is initially at 30 K and magnetized by 7 T, decreasing the magnetic field adiabatically to zero causes the sample temperature drop to 19.5 K. The lower the T_i, the lower is the T_f. An adiabatic removal of magnetic field from $T_i = 20(5\ \text{K})$ leads to $T_f = 5(0.17\ \text{K})$. For comparison of the magnetocaloric properties of $EuTiO_3$ with other materials, we list the maximum values of $-\Delta S$, ΔT_{ad}, RC, and the magnetic transition temperature for other potential magnetic refrigerant materials having a phase transition below 40 K along with $EuTiO_3$ in Table I. EuO and $DyTiO_3$ have a magnetic ordering temperature above 40 K. It can be noted that ΔT_{ad} observed in $EuTiO_3$ is higher than other promising magnetocaloric materials for refrigeration from 1 to 40 K [14,22–29]. Only the metal-organic framework material $Gd(HCOO)_3$ shows a comparable value [29]. Therefore, $EuTiO_3$ has a great potential as a refrigerant material below 40 K.

IV. SUMMARY

In summary, we have studied the magnetocaloric properties of single and polycrystalline $EuTiO_3$ samples using magnetization and heat capacity measurements. A large adiabatic temperature change of 21 K, isothermal entropy change of 49 $\text{J kg}^{-1}\ \text{K}^{-1}$, and a refrigeration capacity of 500 J kg^{-1} for a field change of 7 T were found around the Néel temperature. This compound also shows a remarkable magnetocaloric effect even in low magnetic fields ($\Delta T_{ad} = 5\ \text{K}, -\Delta S = 9\ \text{J kg}^{-1}\text{K}^{-1}$, and $\text{RC} = 33\ \text{J kg}^{-1}$ for $\mu_0 \Delta H = 1\ \text{T}$). Our results suggest that the $EuTiO_3$ could be a potential material for cryogenic magnetic refrigeration below 40 K.

ACKNOWLEDGMENTS

R.M. acknowledges the support of MOE Tier 1 Grant No. R144-000-308-112. J.-S.W. acknowledges the support of MOE Tier 2 Grant No. R144-000-349-112. M.E. acknowledges financial support from MINECO through Grant No. FEDER-MAT2012-38318-C03-01.

APPENDIX: MEAN FIELD CALCULATION FOR $EuTiO_3$

The magnetic model used to describe the $EuTiO_3$ system is a standard Heisenberg model, and its Hamiltonian is given by [20]

$$H = -\sum_{\langle ij \rangle} J_1\, \vec{s}_i \cdot \vec{s}_j - \sum_{[ij]} J_2\, \vec{s}_i \cdot \vec{s}_j - g\mu_B \vec{B} \cdot \sum_i S_i, \tag{A1}$$

where $\langle ij \rangle$ denote the summations over nearest neighbors, and $[ij]$ denote the summations over next nearest neighbors.

In order to apply the mean field approximation, we separated the lattice into two sublattices (a) and (b) (see Fig. 5). It can be seen that the nearest neighbors of site (a) are site (b), the next nearest neighbors of site (a) are site (a) again, and vice versa for site (b). Accordingly, the Hamiltonian (A1) can be separated into Hamiltonian of lattice (a) and Hamiltonian of lattice (b), given by

$$H = H_a + H_b, \tag{A2}$$

where

$$H_a = -\vec{F}_a \cdot \vec{s}_a, \quad H_b = -\vec{F}_b \cdot \vec{s}_b. \tag{A3}$$

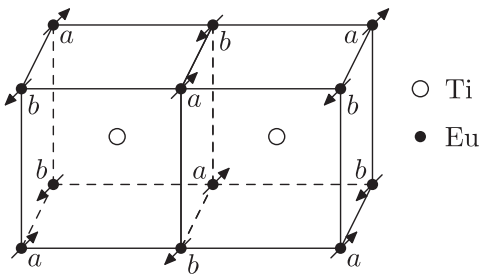

FIG. 5. Schematic representation of the crystal structure for $EuTiO_3$, where (a) and (b) show different magnetic sites of Eu^{2+} ions.

Here, $\vec{F}_a$ and $\vec{F}_b$ are the effective fields for site (a) and site (b), respectively; they are related to the average spin of a site $\vec{s}_a$ and $\vec{s}_b$ by

$$\begin{aligned}\vec{F}_a &= 6J_1\ \langle\vec{s}_b\rangle + 12J_2\ \langle\vec{s}_a\rangle + g\mu_B\vec{B},\\ \vec{F}_b &= 6J_1\ \langle\vec{s}_a\rangle + 12J_2\ \langle\vec{s}_b\rangle + g\mu_B\vec{B}.\end{aligned} \tag{A4}$$

The reason for factor 6 and 12 is that each site has six nearest neighbors and 12 next nearest neighbors.

Equation (A3) can be written in component form:

$$\begin{aligned}H_a &= -\vec{F}_a^x\cdot\vec{s}_a^x - \vec{F}_a^y\cdot\vec{s}_a^y - \vec{F}_a^z\cdot\vec{s}_a^z,\\ H_b &= -\vec{F}_b^x\cdot\vec{s}_b^x - \vec{F}_b^y\cdot\vec{s}_b^y - \vec{F}_b^z\cdot\vec{s}_b^z.\end{aligned} \tag{A5}$$

From standard quantum mechanics we know that the matrix elements for the spin operator are

$$\begin{aligned}\langle\sigma|s_x|\sigma-1\rangle &= \langle\sigma-1|s_x|\sigma\rangle = \frac{1}{2}\sqrt{(s+\sigma)(s-\sigma+1)},\\ \langle\sigma|s_y|\sigma-1\rangle &= \langle\sigma-1|s_y|\sigma\rangle = \frac{-i}{2}\sqrt{(s+\sigma)(s-\sigma+1)},\\ \langle\sigma|s_z|\sigma\rangle &= \sigma.\end{aligned} \tag{A6}$$

Here, σ are the spin indices and $S = 7/2$ is the spin of the Eu^{2+} ion.

Let E_n be the eigenvalue of the Hamiltonian and $|n\rangle$ be the corresponding eigenvector; we have the probability

$$\omega_n = \frac{1}{Z}e^{-\frac{E_n}{k_BT}}, \tag{A7}$$

where Z is the partition function. Thus the average spin of a site is

$$\langle s\rangle = \sum_n \omega_n\langle n|\vec{s}|n\rangle, \tag{A8}$$

in component form

$$\begin{aligned}\langle s_x\rangle &= \sum_n \omega_n\langle n|\vec{s}_x|n\rangle,\\ \langle s_y\rangle &= \sum_n \omega_n\langle n|\vec{s}_y|n\rangle,\\ \langle s_z\rangle &= \sum_n \omega_n\langle n|\vec{s}_z|n\rangle.\end{aligned} \tag{A9}$$

Equations (A4) and (A8) together form a system of self-consistent equations; by iteration, we can find the numerical solutions.

These formulas hold for both sites (a) and (b). Therefore, the formulas for magnetization and entropy are

$$M = g\mu_B\left|\left|\frac{\vec{s}_a+\vec{s}_b}{2}\right|\right|,\quad S = -\frac{1}{2}\sum_n(\omega_{a,n}\ln\omega_{a,n}+\omega_{b,n}\ln\omega_{b,n}), \tag{A10}$$

where $\omega_{a,n}$ denote ω_n for site (a) and $\omega_{b,n}$ denote ω_n for site (b). Note that M and S are functions of T and B implicitly.

Accordingly, we can get the numerical value of the magnetic susceptibility at temperature T by

$$\chi = \frac{M(\Delta B,T) - M(0,T)}{\Delta B}. \tag{A11}$$

The entropy change for different B is

$$\Delta S = S(B,T) - S(0,T), \tag{A12}$$

while the entropy change for different T is

$$\Delta S = S(B,T) - S(B,0). \tag{A13}$$

[1] K. A. Gschneidner, Jr., V. K. Pecharsky, and A. O. Tsokol, Rep. Prog. Phys. **68**, 1479 (2005), and references therein.

[2] A. M. Tishin, in *Handbook of Magnetic Materials*, edited by K. H. J. Buschow (Elsevier, Amsterdam, 1999), Vol. 12, pp. 395–524.

[3] V. Provenzano, J. Li, T. King, E. Canavan, P. Shirron, M. J. Dipirro, and R. D. Shull, J. Magn. Magn. Mater. **266**, 185 (2003).

[4] H. Wada and Y. Tanabe, Appl. Phys. Lett. **79**, 3302 (2001).

[5] J. Liu, T. Gottschall, K. P. Skokov, J. D. Moore, and O. Gutfleisch, Nat. Mater. **11**, 620 (2012).

[6] D. Choudhury, T. Suzuki, D. Okuyama, D. Morikawa, K. Kato, M. Takata, K. Kobayashi, R. Kumai, H. Nakao, Y. Murakami *et al.*, Phys. Rev. B **89**, 104427 (2014).

[7] M. Phan and S. Yu, J. Magn. Magn. Mater. **308**, 325 (2007).

[8] V. Scagnoli, M. Allieta, H. Walker, M. Scavini, T. Katsufuji, L. Sagarna, O. Zaharko, and C. Mazzoli, Phys. Rev. B **86**, 094432 (2012).

[9] T. R. McGuire, M. W. Shafer, R. J. Joenk, H. A. Halperin, and S. J. Pickart, J. Appl. Phys. **37**, 981 (1966).

[10] T. Katsufuji and H. Takagi, Phys. Rev. B **64**, 054415 (2001).

[11] J. H. Lee, L. Fang, E. Vlahos, X. Ke, Y. W. Jung, L. F. Kourkoutis, J. W. Kim, P. J. Ryan, T. Heeg, M. Roeckerath, V. Goian, M. Bernhagen, R. Uecker, P. C. Hammel, K. M. Rabe, S. Kamba, J. Schubert, J. W. Freeland, D. A. Muller, C. J. Fennie, P. Schifer, V. Gopalan, E. Johnston-Halperin, and D. G. Schlom, Nature (London) **466**, 954 (2010).

[12] J. Schiemer, L. J. Spalek, S. S. Saxena, C. Panagopoulous, T. Katsufuji, and M. A. Carpenter, Europhys. Lett. **109**, 57004 (2015).

[13] P. Reuvekamp, K. Caslin, Z. Guguchia, H. Keller, R. K. Kremer, A. Simon, J. Köhler, and A. Busmann-Holder, J. Phys.: Condens. Matter. **27**, 262201 (2015).

[14] K. Rubi, P. Kumar, D. V. M. Repaka, R. Chen, J.-S. Wang, and R. Mahendiran, Appl. Phys. Lett. **104**, 032407 (2014).

[15] Z. J. Mo, J. Shen, L. Li, Y. Liu, C. C. Tang, F. X. Hu, J. R. Sun, and B. G. Shen, Mater. Lett. **158**, 282 (2015).

[16] Z. J. Mo, Z. H. Hao, J. Shen, L. Li, J. F. Wu, F. X. Hu, J. R. Sun, and B. G. Shen, J. Alloys Compd. **649**, 674 (2015).

[17] http://www.qdusa.com/sitedocs/appNotes/ppms/1085-152.pdf.

[18] A. Busmann-Holder, J. Köhler, R. K. Kremer, and J. M. Law. Phys. Rev. B **83**, 212102 (2011); Z. Guguchia, H. Keller,

J. Köhler, and A. Busmann-Holder, J. Phys:. Condens. Matter. **24**, 492201 (2012).
[19] D. Bhoi, P. Mandal, P. Choudhury, S. Pandya, and V. Ganesan, J. Appl. Phys. **110**, 113722 (2011).
[20] P. J. von Ranke, B. P. Alho, E. P. Nobrega, V. S. R. de Sousa, T. S. T Alvarenga, A. Magnus, G. Carvalho, and N. A. de Oliveira, J. Magn. Magn. Mater. **324**, 1290 (2012).
[21] Y. Su, Y. Sui, J.-G. Cheng, J.-S. Zhou, X. Wang, Y. Wang, and J. B. Goodenough, Phys. Rev. B **87**, 195102 (2013).
[22] K. Ahn, A. O. Pecharsky, K. A. Gschneidner, Jr.,and V. K. Pecharsky. J. Appl. Phys. **97**, 063901 (2004).
[23] K. Ahn, V. K. Pecharsky, and K. A. Gschneidner, Jr., J. Appl. Phys. **106**, 043918 (2009).
[24] D. X. Li, T. Yamamura, S. Nimori, Y. Homma, F. Honda, and D. Aoki, Appl. Phys. Lett. **102**, 152409 (2013).
[25] A. Midya, N. Khan, D. Bhoi, and P. Mandal, Appl. Phys. Lett. **101**, 132415 (2012).
[26] P. J. von Ranke, V. K. Pecharsky, and K. A. Gscheidner, Phys. Rev. B **58**, 12110 (1998).
[27] R. Z. Levitin, V. V. Snegirev, A. V. Kopylov, A. S. Lagutin, and A. Gerber, J. Magn. Magn. Mater. **170**, 223 (1997).
[28] A. C. Sackville Hamilton, G. I. Lampronti, S. E. Rowley, and S. E. Dutton, J. Phys.: Condens. Matter **26**, 116001 (2014).
[29] G. Lorusso, J. W. Sharples, E. Palacios, O. Roubeau, E. K. Brechin, R. Sessoli, A. Rossin, F. Tuna, E. J. L. McInnes, D. Collison, and M. Evangelisti, Adv. Mater. **25**, 4653 (2013).